Acta Oceanol. Sin., 2022, Vol. 41, No. 2, P. 15–25
https://doi.org/10.1007/s13131-021-1941-9
http://www.aosocean.com
E-mail: ocean2@hyxb.org.cn

Temporal-spatial oceanic variation in relation with the three typical Kuroshio paths south of Japan

Xiaobo Wu[1], Yanling Zhao[2], Guijun Han[1]*, Wei Li[1, 3]*, Qi Shao[1, 3], Lige Cao[1], Chaoliang Li[1]

[1] School of Marine Science and Technology, Tianjin University, Tianjin 300072, China

[2] The PLA 31010 Units, Beijing 100081, China

[3] Tianjin Key Laboratory for Oceanic Meteorology, Tianjin 300074, China

Received 24 May 2021; accepted 3 September 2021

Abstract

Empirical orthogonal function (EOF) analysis was applied to a 50-year long time series of monthly mean positions of the Kuroshio path south of Japan from a regional reanalysis. Three leading EOF modes characterize the contributions from three typical paths of the Kuroshio meander: the typical large meander path, the offshore non-large meander path, and the nearshore non-large meander path, respectively. Accordingly, the spatial variation characteristics of oceanic anomaly fields can be depicted by their regression fields upon the associated three leading principal components (PCs), which are well-matched with the results of composite analysis corresponding to each period of the three typical Kuroshio paths. A new index for the typical large meander is defined by using the second leading PC, which is highly correlated with the Kushimoto-Uragami index. Spectral analysis of this new index series shows variability of the Kuroshio path south of Japan at time scales of about 7–8 years and 20 years.

Key words: Kuroshio path, south of Japan, empirical orthogonal function analysis, temporal-spatial oceanic variation, large meander index

Citation: Wu Xiaobo, Zhao Yanling, Han Guijun, Li Wei, Shao Qi, Cao Lige, Li Chaoliang. 2022. Temporal-spatial oceanic variation in relation with the three typical Kuroshio paths south of Japan. Acta Oceanologica Sinica, 41(2): 15–25, doi: 10.1007/s13131-021-1941-9

1 Introduction

The Kuroshio is the western boundary current of the wind-driven subtropical circulation system in the North Pacific. It brings heat and nutrients northward, impacting local weathers and climate and shaping marine ecosystems (Nakata et al., 2000; Kelly et al., 2010; Xu et al., 2010; Nakamura et al., 2012; Hayasaki et al., 2013). It is well known that when the Kuroshio heads eastward along the southern coast of Japan, it takes one of the three typical paths: typical large meander (tLM) path, offshore non-large meander (oNLM) path, and nearshore non-large meander (nNLM) path (Kawabe, 1985; Fig. 1). The variation of the Kuroshio path south of Japan has always been an important topic due to such distinct features.

Early research mainly focused on the bimodality of the Kuroshio path south of Japan using ocean observation data (Taft, 1972; Nitani, 1975; Kawabe, 1985, 1987, 1995) and modeling (Chao and McCreary, 1982; Chao, 1984; Yamagata and Umatani, 1987, 1989; Awaji et al., 1991). The availability of high-quality satellite dataset since the 1990s marked the beginning of an era in studying the roles of mesoscale eddies in the variation of the Kuroshio path (Mitsudera et al., 2001; Ebuchi and Hanawa, 2003; Sugimoto and Hanawa, 2012; Ma, 2019). Moreover, the development of the ocean models and assimilation techniques, has laid the foundation for exploring actual Kuroshio path variations (Miyazawa et al., 2008; Usui et al., 2008, 2011, 2013) and long-term variations (Douglass et al., 2012; Usui et al., 2013; Tsujino et al., 2013). Miyazawa et al. (2008) used an ocean forecast system called the Japan Coastal Ocean Predictability Experiment, to simulate the formation of Kuroshio large meander in 2004; their results showed that this large meander is caused by baroclinic instability. This mechanism is confirmed by Usui et al. (2008) based on a data assimilation and prediction system of the Meteorological Research Institute Community Ocean Model. Usui et al. (2011) examined the decay mechanism of the 2004/05 Kuroshio large meander based on ocean general circulation model (OGCM), and proposed three mechanisms responsible for the event. Douglass et al. (2012) conducted a long-term global OGCM simulation, and their results indicated that the meander is from intrinsic oceanic variability. Usui et al. (2013) used an ocean data assimilation system to investigate the long-term variability of the Kuroshio path south of Japan, and pointed out that the Kuroshio large meander is closely related to Kuroshio transport. Tsujino et al. (2013) explored the effects of large-scale wind forcing on the Kuroshio path south of Japan using a 60-year historical OGCM simulation, and demonstrated the relationship between the path and Kuroshio transport.

While the trimodality in the Kuroshio path south of Japan has been a hot topic since its recognition in observations (Kawabe, 1985, 1995), observational and modeling studies to date have targeted different states of the path separately, with the large meander receiving more attention. There have been limited studies on the three distinct Kuroshio paths, which address the associated temporal-spatial variations of oceanic anomaly fields simultaneously based on long-term reanalysis datasets. In this study,

Foundation item: The National Natural Science Foundation of China under contract No. 41876014.
*Corresponding author, E-mail: guijun_han@tju.edu.cn; liwei1978@tju.edu.cn

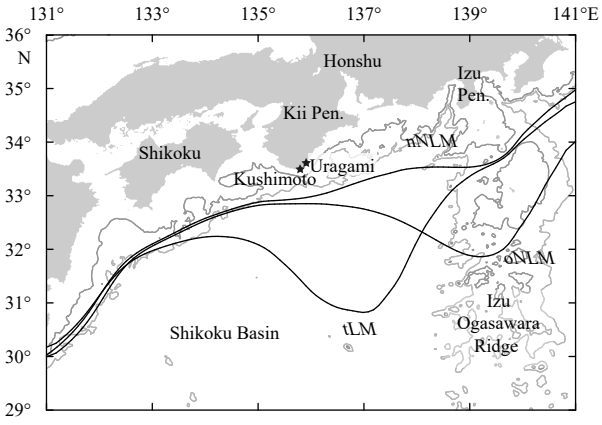

Fig. 1. Three typical Kuroshio paths south of Japan: nearshore non-large meander (nNLM), offshore non-large meander (oNLM), and typical large meander (tLM). The gray contours are isobaths 1 000 m and 2 000 m. The two stars denote Kushimoto and Uragami tide gauge stations.

an ocean reanalysis dataset for the Northwest Pacific with a 50-year time span from 1958 to 2007 is used as the baseline to retrieve the Kuroshio path south of Japan, and to investigate the temporal-spatial variations of ocean state variables in the coastal waters off southern Japan. The rest of the paper is arranged as follows. Data and methods are introduced in Section 2. Analysis results are presented in Section 3, followed by summary and discussion in Section 4.

2 Data and methods

The oceanic reanalysis dataset employed in this study is produced by a regional ocean reanalysis system for the Northwest Pacific, called the China Ocean Reanalysis (CORA; http://www.cmoc-china.cn; Han et al., 2011, 2013). The CORA system assimilated satellite remote sensing sea surface temperature (SST), altimetry sea surface height anomaly (SSHA), and *in situ* temperature/salinity profiles into the parallelized Princeton Ocean Model with a generalized coordinate system (POMgcs; Mellor et al., 2002; Ezer and Mellor, 2004) by using a sequential three-dimensional variational (3D-Var) scheme implemented within a multigrid framework (Li et al., 2008). The daily reanalysis spans 50 years from January 1958 to December 2007. The atmospheric forcing fields used are 0.25° daily wind from the cross-calibrated multi-platform (Atlas et al., 2011), combining 6-hourly wind at 1.875° and heat and water fluxes from the National Centers for Environmental Prediction and the National Center for Atmospheric Research (NCEP-NCAR; Kalnay et al., 1996) reanalysis. Considering the tidal mixing effect on the formation of tidal front in the coastal region, a tidal open boundary condition was introduced into the CORA system. The horizontal resolution of the CORA reanalysis data for the Kuroshio south of Japan is 0.25°. A total of 35 hybrid vertical coordinate surfaces is employed by combining sigma and z-level. Throughout the rest of this paper, this regional ocean reanalysis dataset is called the CORA data. Based on the CORA data, the three typical Kuroshio paths south of Japan are obtained (see Section 3.1 for the classification of the typical Kuroshio paths) and shown in Fig. 1. The daily time series of the latitude of Kuroshio path is then obtained from the CORA data by defining a specific sea surface height (SSH) isoline of 70 cm as the axis (Qiu and Chen, 2005; Sugimoto and Hanawa, 2012).

To examine the skill of the CORA data in the study area (29°–36°N, 131°–141°E), the daily absolute dynamic topography (ADT) data of the Ssalto/Duacs altimeter products during January 1993 to December 2007 from the Copernicus Marine and Environment Monitoring Service (CMEMS) (https://marine.copernicus.eu) is used as a reference. The monthly time series of the southernmost latitude of the Kuroshio path between 136°E and 140°E is also used, which is produced by the Japan Meteorological Agency (JMA) based on the temperature at the depth of 200 m and satellite-derived SST data (Sugimoto et al., 2020), hereinafter the JMA data. The JMA data can be obtained at http://www.data.jma.go.jp/kaiyou/data/shindan/b_2/kuroshio_stream/kuro_slat.txt. It is worth noting that 110 cm ADT isoline is used to define the axis as the reference mean sea surface employed in the altimetry data is different from that of the CORA data.

Figure 2 provides the validation of the CORA data (blue solid line) against both the altimetry observations (red solid line) and JMA data (black dashed line). It can be seen that the CORA data well capture the observed monthly averaged axis positions between 136°E and 140°E. The correlation coefficients of the CORA data with the altimetry and JMA data exceed 0.90, with a 99% confidence level; hereafter all correlations mentioned in this study are significant with the 99% confidence level.

The degree of fidelity of the CORA data can be further demonstrated by comparing to the altimetry data during 2004/05 tLM event, which is the first tLM event since the altimetry data became available in 1993, and to the sea-level difference between Kushimoto and Uragami obtained by using 43 years (1965–2007) monthly mean sea-level observational data from the Permanent Service for Mean Sea Level (PSMSL) (https://www.psmsl.org; Holgate et al., 2013). The comparison confirms that the CORA data used in this study can be considered as a competent candidate for exploring the variation of the Kuroshio in this region (see Section 3.3 for detail).

For analysis, the empirical orthogonal function (EOF) analysis is used, which is a method of decomposition of a signal in terms of orthogonal basis functions, same as performing a principal components analysis (PCA) on the data (Hannachi et al., 2007). It has been adopted to investigate the tempo-spatial variation of ocean state variables related to the Kuroshio (Yasuda and Sakurai, 2006; Wei et al., 2013; Wang and Oey, 2014, 2016).

In this study, the main focus is the variability of the Kuroshio path south of Japan at the interannual time scale and beyond. Based on the 50-year daily time series of the Kuroshio path extracted from the CORA data with the axis position represented by latitude with 0.25° longitude resolution between 131°E and 141°E,

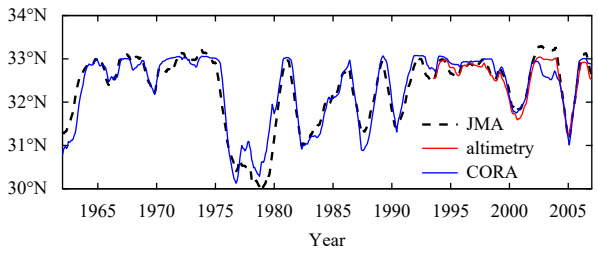

Fig. 2. Time series from January 1961 to December 2007 of the monthly averaged southernmost latitude of the Kuroshio path south of Japan from the Japan Meteorological Agency (JMA, black dashed line), altimetry (red solid line), and China Ocean Reanalysis (CORA, blue solid line) data. All three time series are lowpass-filtered using 13-month running mean. The correlation coefficients of the CORA data with the altimetry and JMA data all exceed 0.90.

the corresponding monthly mean time series was calculated and then a 13-month lowpass filter was applied. The EOF analysis was performed to the anomalies of the monthly mean axis position by subtracting the climatological monthly means calculated using all 50 years of the data.

3 Results

3.1 *Classification of the three Kuroshio paths*

Based on the definition of Sugimoto and Hanawa (2012), the typical Kuroshio paths are defined as follows:

(1) If the average position of the Kuroshio path between 135°E and 136°E is located north of 32°N, the average position of the Kuroshio path between 137°E and 138°E is located north of 32.8°N, and the average position of the Kuroshio path around 140°E is located north of 33.2°N, it is the nNLM path.

(2) If the average position of the Kuroshio path between 135°E and 136°E is located north of 32°N, and the average position of the Kuroshio path around 140°E is located south of 33.0°N, it is the oNLM path.

(3) If the average position of the Kuroshio path between 136°E and 138°E is located south of 32.3°N, it is the tLM path.

According to the above classification, the numbers of monthly mean paths for nNLM, oNLM, and tLM are 110 (18.3%), 244 (40.7%), and 150 (25%), respectively. The remaining 96 paths (10%), called the "others" when the Kuroshio takes an undulated path that is not regarded as any of the three typical paths, represent the transitioning paths of the Kuroshio, which is not considered in this study.

3.2 *EOF analysis*

By performing EOF analysis on the 50-year monthly mean time series of the Kuroshio path, the EOF modes (i.e., spatial patterns) and their corresponding principal components (PCs) (i.e., temporal coefficients) were obtained. All the modes pass the significant test (North et al., 1982). The cumulative fraction of the total variance accounted for by the first three leading EOF modes is listed in Table 1, which contribute more than 91% of the total variance.

The spatial distributions of the first three EOF modes are shown in Fig. 3. The first leading EOF mode (EOF1) accounts for 46.26% of the total variance, with a negative (southward) curve between 138°E and 141°E (solid line). Such spatial distribution of EOF1 resembles the oNLM path south of Japan. EOF2, with a positive curve between 136°E and 138°E (dashed line), accounts for 28.23% of the total variance. The spatial distribution of EOF2 with the curve being regarded as the corresponding southward meander is similar to the tLM path. Finally, 16.71% of the total variance is accounted for by EOF3. There is a similarity between EOF3 with all spatial values being positive (northward) and the nNLM path (dash-dotted line).

Table 1. Cumulative proportions of the EOF modes

EOF mode	Explained variance/%	Cumulative explained variance/%
1	46.26	46.26
2	28.23	74.49
3	16.71	91.21

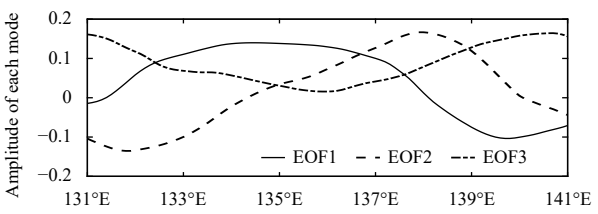

Fig. 3. Spatial distributions of EOF1 (solid line), EOF2 (dashed line), and EOF3 (dash-dotted line). EOF, empirical orthogonal function.

Figure 4 displays the temporal coefficients corresponding to the first three leading EOF modes. As shown in Fig. 4a, the oNLM events mostly correspond to positive values of PC1. The typical Kuroshio large meander periods, occurred in 1959–1963, 1981–1984, 1986–1988, 1989–1990, and 2004–2005, respectively, well matched with all negative peaks of PC2 in Fig. 4b. It seems that the amplitude of PC2 needed to be larger than 0.35 (as a threshold) when the Kuroshio large meander occurred. For instance, the amplitude of PC2 was only about 0.2 around 2000, during which no large meander occurred. Similarly, most positive peaks of PC3 are in the nNLM periods.

In summary, it seems that the first three leading modes of the EOF and their corresponding temporal coefficients reflect the characteristics of the three typical Kuroshio paths. Next, the physical meaning of each leading mode in terms of the three typical Kuroshio paths is searched by exploring these spatial patterns and time series signals.

3.3 *Spatial variation characteristics of anomaly fields*

In this section, regression analysis is employed to explore the spatial variations of anomaly fields of SSH, SST, sea surface salinity (SSS), 200-m depth temperature, and 200-m depth salinity in the study region, namely, SSHA, SSTA, SSSA, 200TA, and 200SA. The regression coefficient fields of these variables are obtained by regressing their anomaly fields onto PC1, PC2, and PC3, respectively. Composite analysis is used to examine the regression results. Comparison between the regression maps and composite anomalies can confirm the previous interpretation of the contributions of the three typical Kuroshio paths to the first three leading EOF modes.

3.3.1 *Regression and composite analyses associated with PC1*

The regression fields for all the five ocean variables with respect to PC1 are depicted in the left panels of Fig. 5. All the regression fields mainly present a dipole pattern with its center being symmetrical along the northeast–southwest (NE–SW) direc-

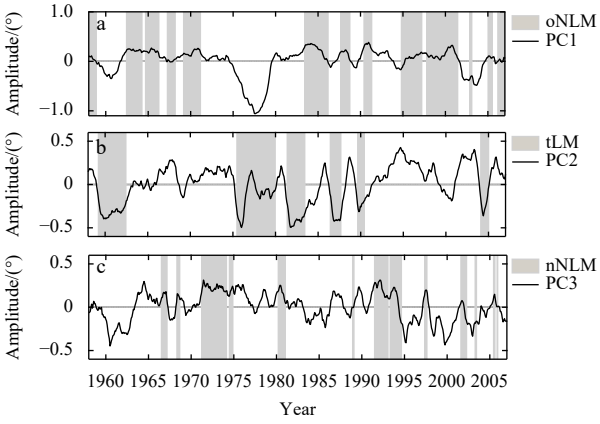

Fig. 4. Time series corresponding to EOF1 (a, PC1), EOF2 (b, PC2), and EOF3 (c, PC3). Shadings represent the periods of oNLM, tLM, and nNLM, respectively.

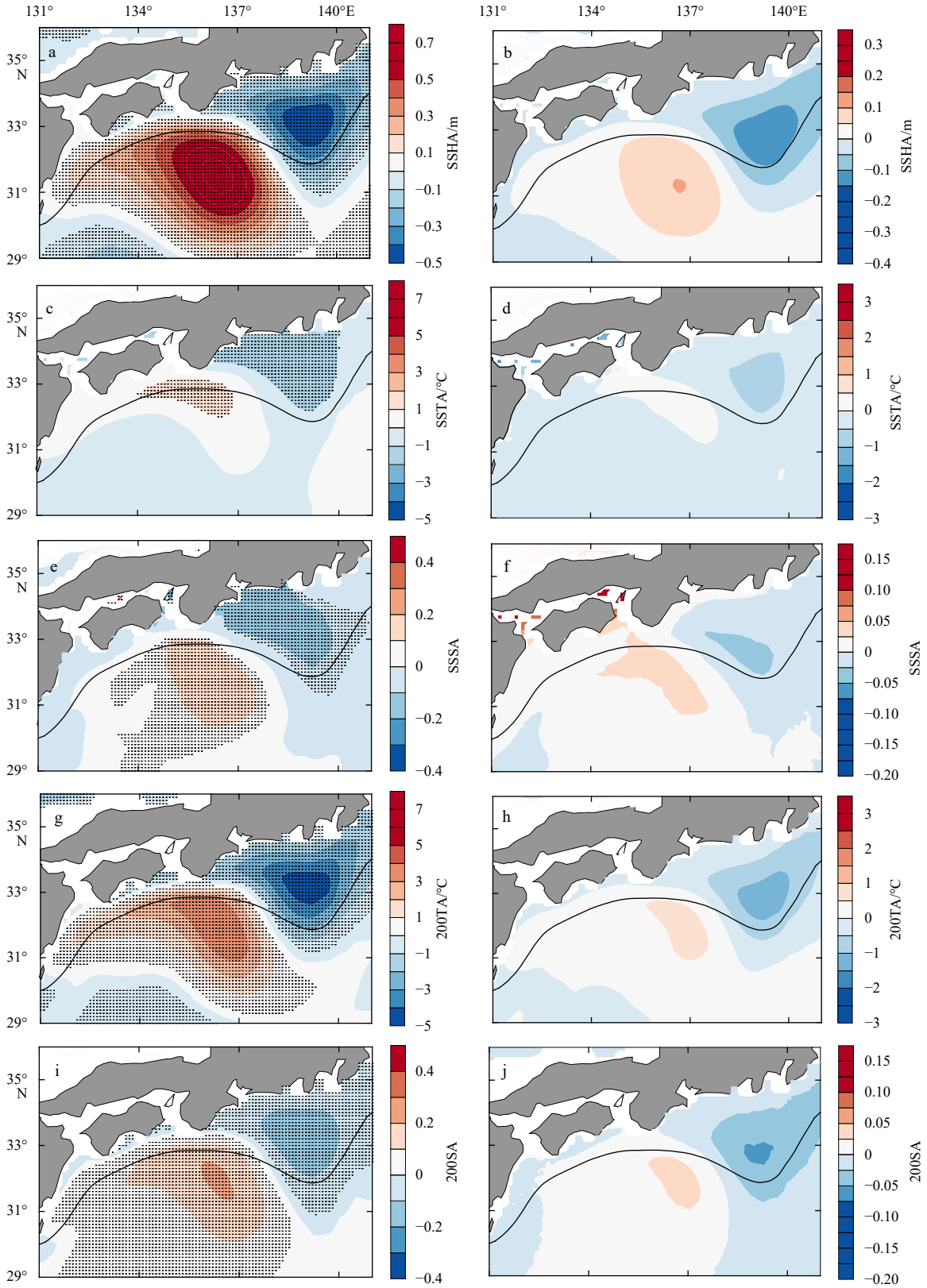

Fig. 5. Left panels: regression fields of sea surface height anomaly (SSHA) (a), sea surface temperature anomaly (SSTA) (c), sea surface salinity anomaly (SSSA) (e), 200-m depth temperature anomaly (200TA) (g), and 200-m depth salinity anomaly (200SA) (i) upon PC1. Stippling indicates exceeding the 95% significance level. Right panels: composite maps of SSHA (b), SSTA (d), SSSA (f), 200TA (h), and 200SA (j) in the oNLM period. The thick black line shows the oNLM path.

tion. The positive anomaly center is located south of the Kii Peninsula, and the negative anomaly center appears downstream of the positive one. The positive and negative anomaly areas are located on offshore and inshore sides of the Kuroshio path, re-

spectively. During the oNLM period, each composite field of SSHA, SSSA, 200TA, and 200SA (right panels in Fig. 5) shows the same dipole pattern. For the composite SSTA field (Fig. 5d) with the dipole absent, there is only a negative anomaly center, but not obvious in strength or range. The dipoles produced by the regression being the same in strength and spatial structure with the composite can be the evidence that the first leading EOF mode is contributed by the oNLM path.

According to previous studies, such dipole distribution in the regression field is due to an anticyclonic circulation, i.e., the Shikoku Recirculation Gyre (SRG), located to the south of the Kuroshio in the Shikoku Basin (Sugimoto et al., 1986; Mitsudera et al., 2006). Following Qiu and Chen (2005) and Li et al. (2014), the formula below is employed to calculate the strength of SRG using the CORA data.

$$S(t) \equiv \iint_A h(x, y, t)\,\mathrm{d}x\mathrm{d}y, \tag{1}$$

where A denotes the area with SSH>0.9 m in the region of 30°–33.5°N, 132°–140°E.

As shown in Fig. 6a, when the Kuroshio transitions to the oNLM path, the SRG strength increases, which leads to positive oceanic anomalies south of the Kii Peninsula (Qiu and Miao, 2000; Li et al., 2014). At the same time, a cyclonic circulation, associated with the large meander, propagates eastward to the south of the Izu Peninsula, resulting in negative oceanic anomalies. Taking the 2004/05 tLM event as an example, Figs 7c and d describe the time evolution of SSH and its anomaly obtained from the first 10-day mean in each month using the CORA and altimetry data during the decay period (from April to September 2005; see Usui et al., 2011). The eastward propagation process of the negative oceanic anomalies can be clearly observed in both CORA and altimetry data, which match each other well.

3.3.2 *Regression and composite analyses associated with PC2*

As shown in the left panels of Fig. 8, the manifestation for each of the regression fields of SSHA, SSSA, 200TA, and 200SA (Figs 8a, e, g, and i) upon PC2 is a spatially asymmetric dipole pattern but exhibiting the same orientation of NE–SW with that for PC1. The negative anomaly area has a greater amplitude and range than the positive one for each of these four variables. The range of the negative anomaly area stretches across the mean path of the Kuroshio large meander, with a notable center located between the inshore side of the Kuroshio path and the southern coast of Honshu. Meanwhile, the relatively weak positive anomaly center exists on the inshore side of the Kuroshio path. Although the regression field of SSTA (Fig. 8c) also presents the same NE–SW oriented dipole pattern, it is weak in strength and small in range in contrast to the other four variables. This situation is just like regression field upon PC1, the negative regression center at 200-m depth (Fig. 8e), comparing with that of SSTA (Fig. 8c), is both strengthened and enlarged in range with the negative center moving southward from the inshore side of the Kuroshio path to coincide with the mean state of the path, while the positive center is clearly presented downstream of the negative one. Comparatively speaking, the positive regression field of 200SA (Fig. 8i) exhibits the same spatial pattern with that of SSSA (Fig. 8e) as those upon PC1. This similarity in spatial pattern is demonstrated between the regression fields upon PC2 and the composite anomaly fields in the tLM periods (see the right panels of Fig. 8), except the positive and negative centers are exactly the opposite. Thus, it indicates that EOF2 is contributed by the Kuroshio large meander path.

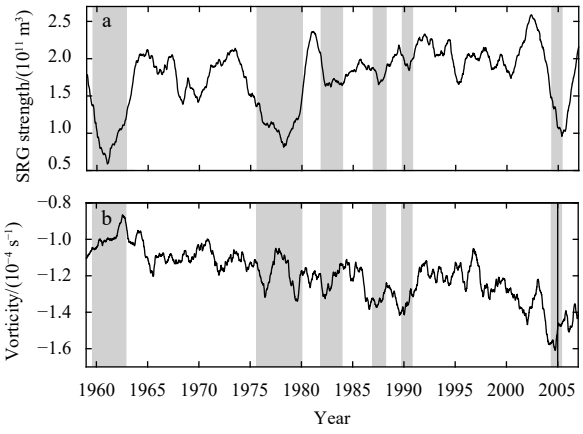

Fig. 6. Time series of the Shikoku Recirculation Gyre (SRG) strength (a) and relative vorticity averaged in the upper 500 m (b) in the region of 30°–33.5°N, 132°–140°E. Both time series are low-pass-filtered using 13-month running mean. Shading indicates tLM periods.

The oceanic anomalies revealed by both regression and composite are confirmed by modeling results for individual large meander events (Douglass et al., 2012; Tsujino et al., 2013). Figures 7a and b depict the time evolution of SSH and its anomaly obtained from the first 10-day mean in each month using the CORA and altimetry data during the 2004/05 Kuroshio large meander formation period (from March to August 2004; see Miyazawa et al., 2008; Usui et al., 2008). It shows that an accompanying anticyclonic eddy with the trigger meander (a small-scale meander first appears off the southeast of Kyushu (Solomon, 1978; not shown here) and then grows during its eastward propagation, resulting in the tLM; see Usui (2019) was developed on the opposite side of the Kuroshio path and the positive anomaly was advected downstream until the large meander blocked it and hence the anomaly accumulated there. By comparison, during the formation process of the large meander (Figs 7a and b) the CORA data do not match the altimetry data as well as during the decay process (Figs 7c and d).

3.3.3 *Regression and composite analyses associated with PC3*

The regression fields of SSHA, SSTA, SSSA, 200TA, and 200SA upon PC3 (left panels in Fig. 9) are mainly characterized by a large positive area to the south of Honshu, with the center appearing at the offshore side of the Kuroshio path. Meanwhile, all these regression fields display weak negative anomalies in the southern coastal areas of Honshu. The composite anomaly fields of these five variables related to the nNLM path (right panel in Fig. 9) are well matched in spatial patterns with the regression fields upon PC3, which hints that the nNLM path of the Kuroshio contributes to EOF3.

The following mechanism is attributed to such characteristics of the anomaly fields: when the Kuroshio is in the period of the non-large meander, the current continuously transports low-potential vorticity (PV) water from the upstream of the Kuroshio south of Japan and accumulates it in the region south of Japan, resulting in the strengthening of the SRG (Qiu and Miao, 2000; Li et al., 2014; Usui, 2019) and a huge positive anomaly region on the offshore side of the Kuroshio south of Japan. Following Qiu and Miao (2000), the averaged relative vorticity ($\zeta = \partial v/\partial x -$

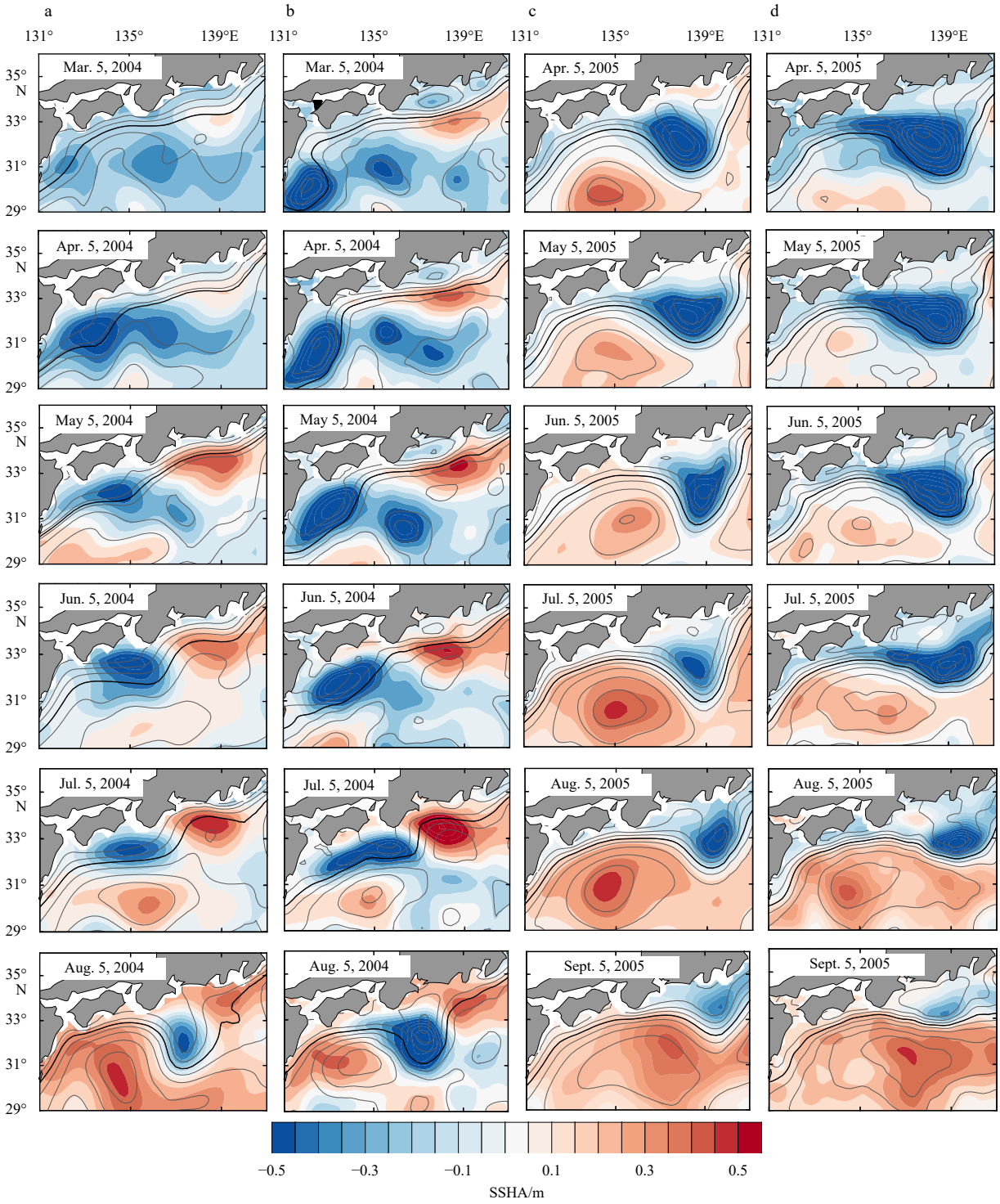

Fig. 7. Month-by-month SSH (contour with 0.2 m interval) and SSHA (shading) obtained from the first 10-day mean for each month using the CORA (a, c) and altimetry (b, d) data during March–August 2004 (a, b) and during April–September 2005 (c, d). The thick black line denotes the Kuroshio axis.

$\partial u/\partial y$) over the upper 500 m in the region of (30.0°–33.5°N, 132°–140°E) is calculated by using the CORA data. As shown in Fig. 6b, a decreasing trend of the relative vorticity is captured in the nNLM path (e.g., 1985–1986, 1988–1989), which denotes the accumulation of low-PV anomalies south of Japan. At the same time, the strength of the SRG is larger compared to that in the tLM period (see Fig. 6a).

In summary, the spatial patterns of SSTA illustrated by regression in this study are essentially in agreement with those illustrated in Sugimoto et al. (2020) using the multiscale ultrahigh-resolution SST product from 2003 to 2018 with a horizontal resolution of 1 km developed by the NASA Jet Propulsion Laboratory. Especially the regression map of SSTA upon PC2 is matched well with that in Sugimoto et al. (2020), which was obtained from the ERA5 SST data for the six events of large meander since 1975. At the same time, in their paper the coastal warming off the Tokai

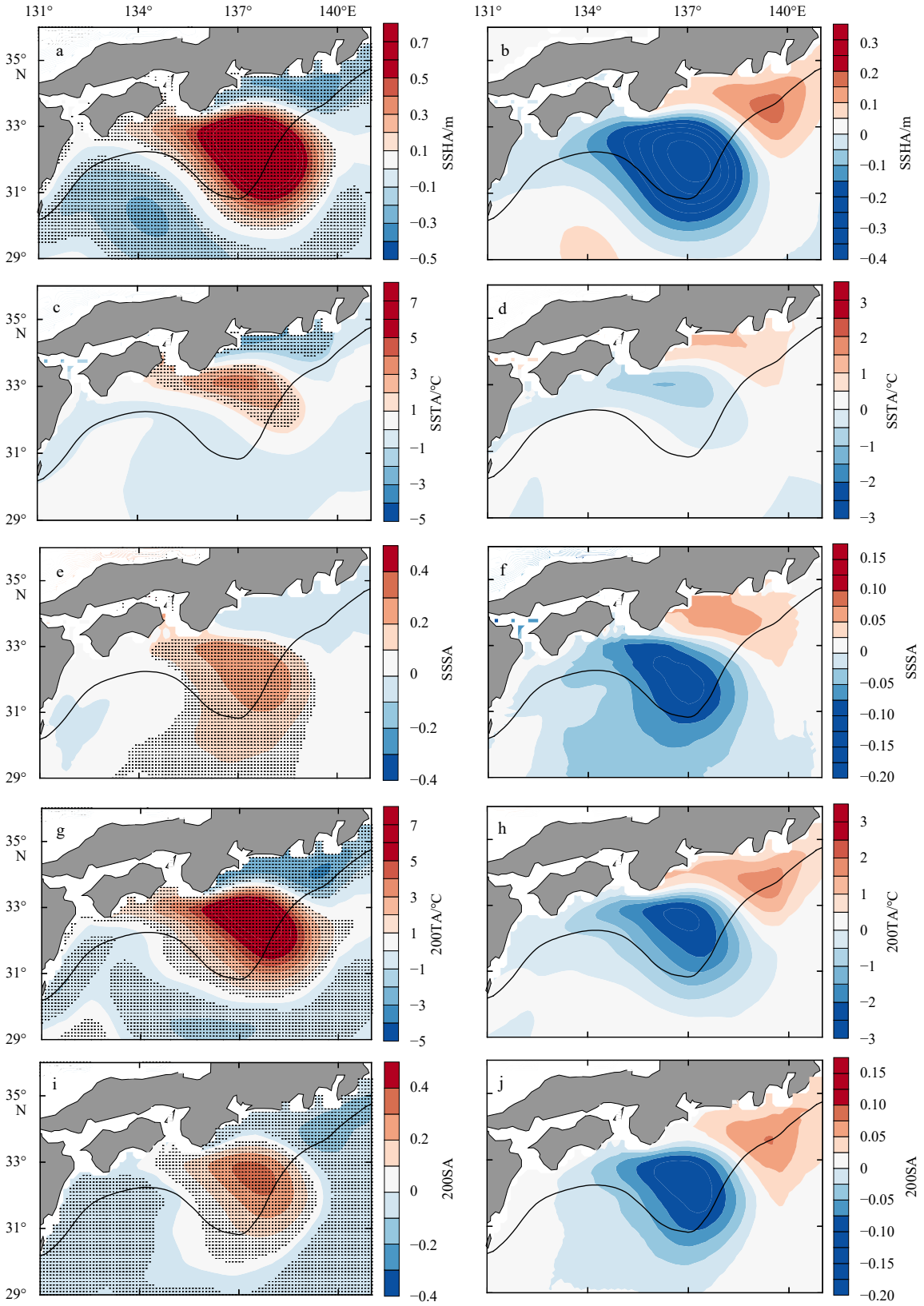

Fig. 8. Left panels: regression fields of SSHA (a), SSTA (c), SSSA (e), 200TA (g), and 200SA (i) upon PC2. Stippling indicates exceeding the 95% significance level. Right panels: composite maps of SSHA (b), SSTA (d), SSSA (f), 200TA (h), and 200SA (j) in the tLM period. The thick black line shows the tLM path.

district at 200-m depth during the tLM period was confirmed in the temperature profiles archived in the World Ocean Database 2018, which is in good agreement with the regression map of 200TA. Since the regression fields upon the first three PCs reveal-

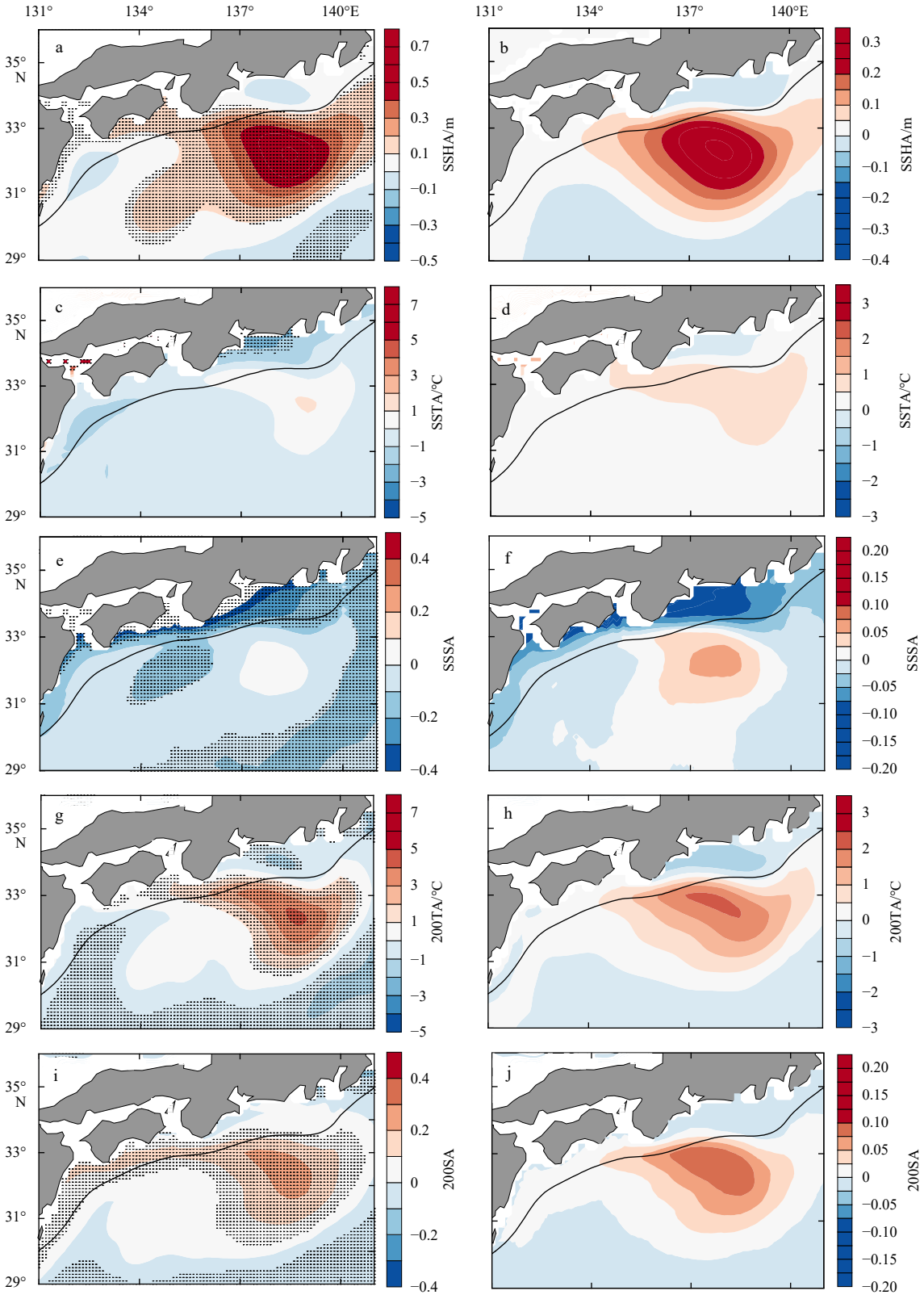

Fig. 9. Left panels: regression fields of SSHA (a), SSTA (c), SSSA (e), 200TA (g), and 200SA (i) upon PC3. Stippling indicates exceeding the 95% significance level. Right panels: composite maps of SSHA (b), SSTA (d), SSSA (f), 200TA (h), and 200SA (j) in the nNLM period. The thick black line shows the nNLM path.

ing the spatial anomaly distribution characteristics of the ocean variables are consistent with the composite maps of SSH and thermohaline anomalies in the Kuroshio region south of Japan, it can thus be concluded that contributions of the three typical paths can be separated into the first three leading EOF modes, respectively.

3.4 *A new index to detect the Kuroshio large meander*

It has been found that the sea-level difference between Kushimoto and Uragami depicts the Kuroshio variation around the Kii Peninsula by exhibiting relatively small (large) in large meander (non-large meander) periods (Kawabe, 1995; Sekine and Fujita, 1999) and gives an excellent index of the large meander (abbreviated as the KUI) (Nakamura et al., 2012; Miyama and Miyazawa, 2013). The temporal variation of PC2 (solid line) against the monthly mean time series of the KUI (dashed line) is illustrated in Fig. 10. The correlation coefficient of the two time series is as high as 0.78. As can be seen in Fig. 10, the normalized PC2 matches well with the KUI during the large meander years except for the meander of 1975–1980. The reason may lie in the fact that there was a short period of northward shift of the Kuroshio path in 1978; and a significant northward overshoot (about half degree) was found in the reconstruction of the Kuroshio path from the CORA system (see the blue solid line in Fig. 2). Consequently, the southernmost positions of the Kuroshio path cannot be reproduced correctly either by the CORA system right after that short period of northward shift. However, the similarity between PC2 and KUI implies that PC2 can be defined as a new Kuroshio large meander index.

Following the wavelet analysis method described in Torrence and Compo (1998), the Morlet wavelet transform was applied to the time series of PC2 and the JMA data. Then, the global wavelet spectrum, which is the time average of the wavelet power spectrum (Farge, 1992; Nakamura et al., 2006), can be achieved. As shown in Fig. 11, periods of about 7–8 years and 20 years present in the spectra of PC2 and the JMA data, with the significance exceeding the 95% confidence level for a red-noise process. The variability of the Kuroshio path south of Japan on such time scales was reported in previous studies. For instance, Nitani (1975) concluded that the long-term variation of the Kuroshio south of Japan exhibits a period of 7–9 years. Kawabe (1987) also pointed out that the Kuroshio large meander has periods of about 7–8.5 years and 20 years base on his power spectral analysis. Although a period of about 4 years is derived in the spectra of both PC2 and the JMA data, the latter is not statistically significant at the 95% confidence level.

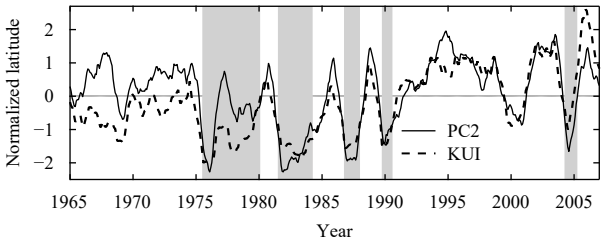

Fig. 10. Normalized time series of PC2 (solid line) and KUI (dashed line). Shading indicates tLM periods.

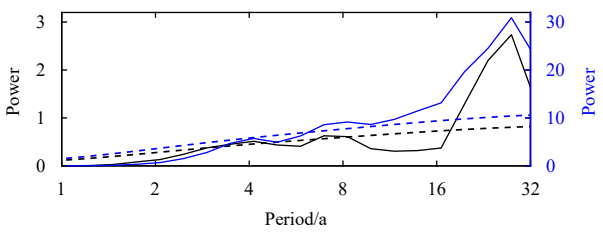

Fig. 11. The global wavelet spectrum of PC2 (black solid line) and the JMA data (blue solid line). The dashed lines represent the 95% confidence level for a red-noise process (α=0.72).

4 Summary and discussion

In this study, the temporal-spatial variations of the Kuroshio path south of Japan and oceanic anomaly fields in the coastal region related to the three typical paths are investigated based on a long time series reconstruction from 1958 to 2007 in the Northwest Pacific by the CORA. The EOF analysis was applied to the latitude deviation of monthly mean axis position of the Kuroshio path south of Japan in the CORA data. Results show that the first three leading EOF modes (EOF1, EOF2, and EOF3) can explain more than 91% of the total variance. A thorough examination through comparing research findings with observations is performed on the results of EOF analysis by using regression and composite analyses. The regression fields upon the first three leading PCs clearly demonstrate the spatial variation patterns of the ocean state variables, including SSH, SST and SSS together with 200-m depth temperature and salinity, which are contributed by the three typical Kuroshio paths; they are in good agreement with the composites. Therefore, it can be concluded that the first three leading EOFs and their corresponding time coefficients (PC1, PC2, and PC3) can be closely linked to the three typical paths taken by the Kuroshio, in which the oNLM path contributes to the EOF1 mode, the tLM path contributes to the EOF2 mode, and the nNLM path contributes to the EOF3 mode, respectively.

Through comparing with the KUI (the sea-level difference between Kushimoto and Uragami), PC2 can be defined as a new index to detect the Kuroshio large meander. A correlation coefficient of 0.78 indicates a strong correlation between PC2 and KUI. Spectral structures of PC2 and the JMA data exhibit variability of the Kuroshio path south of Japan at time scales of about 7–8 years and 20 years.

From this study, it is recognized that there is room for improving the capability of the CORA system in the Kuroshio region. It is definitely a topic worthy of further investigation to achieve the goal of continuously upgrading the CORA system, which has been developed for more than a decade (Han et al., 2011). Another interesting topic as a follow-up study is the prediction of the Kuroshio path south of Japan, which has always been a topic of concern. At present, numerical modeling is still the main method for the prediction of the Kuroshio path south of Japan (Miyazawa et al., 2005; Usui et al., 2006). With the increasing availability of oceanographic observations and ocean reanalysis products with reliable error estimates, extensive applications of various types of artificial neural networks based on deep learning framework have recently been directed to ocean prediction (Zhang et al., 2017; Song et al., 2020). Thus, it motivates us to explore the feasibility of such method in the prediction of the Kuroshio path south of Japan.

Acknowledgements

We thank the Copernicus Marine and Environment Monitoring Service for providing the ADT data (https://resources.marine.copernicus.eu/?option=com_csw& task=results), the Permanent Service for Mean Sea Level for providing the monthly mean sea level data of Kushimoto and Uragami (https://www.psmsl.org/data/obtaining/), and the Japan Meteorological Agency for providing monthly time series of the southernmost latitude of the Kuroshio path between 136°E and 140°E (http://www.data.jma.go.jp/kaiyou/data/shindan/b_2/kuroshio_stream/kuro_slat.txt). We also thank the editor and two anonymous reviewers for their helpful comments to improve the quality of this paper.

References

Atlas R, Hoffman R N, Ardizzone J, et al. 2011. A cross-calibrated,

multiplatform ocean surface wind velocity product for meteorological and oceanographic applications. Bulletin of the American Meteorological Society, 92(2): 157–174, doi: 10.1175/2010BAMS2946.1

Awaji T, Akitomo K, Imasato N. 1991. Numerical study of shelf water motion driven by the Kuroshio: barotropic model. Journal of Physical Oceanography, 21(1): 11–27, doi: 10.1175/1520-0485(1991)021<0011:NSOSWM>2.0.CO;2

Chao S Y. 1984. Bimodality of the Kuroshio. Journal of Physical Oceanography, 14(1): 92–103, doi: 10.1175/1520-0485(1984)014<0092:BOTK>2.0.CO;2

Chao S Y, McCreary J P. 1982. A numerical study of the Kuroshio south of Japan. Journal of Physical Oceanography, 12(7): 679–693, doi: 10.1175/1520-0485(1982)012<0679:ANSOTK>2.0.CO;2

Douglass E M, Jayne S R, Bryan F O, et al. 2012. Kuroshio pathways in a climatologically forced model. Journal of Oceanography, 68(5): 625–639, doi: 10.1007/s10872-012-0123-y

Ebuchi N, Hanawa K. 2003. Influence of mesoscale eddies on variations of the Kuroshio path south of Japan. Journal of Oceanography, 59(1): 25–36, doi: 10.1023/A:1022856122033

Ezer T, Mellor G L. 2004. A generalized coordinate ocean model and a comparison of the bottom boundary layer dynamics in terrain-following and in z-level grids. Ocean Modelling, 6(3–4): 379–403, doi: 10.1016/S1463-5003(03)00026-X

Farge M. 1992. Wavelet transforms and their applications to turbulence. Annual Review of Fluid Mechanics, 24: 395–458, doi: 10.1146/annurev.fl.24.010192.002143

Han Guijun, Li Wei, Zhang Xuefeng, et al. 2011. A regional ocean reanalysis system for coastal waters of China and adjacent seas. Advances in Atmospheric Sciences, 28(3): 682–690, doi: 10.1007/s00376-010-9184-2

Han Guijun, Li Wei, Zhang Xuefeng, et al. 2013. A new version of regional ocean reanalysis for coastal waters of China and adjacent seas. Advances in Atmospheric Sciences, 30(4): 974–982, doi: 10.1007/s00376-012-2195-4

Hannachi A, Jolliffe I T, Stephenson D B. 2007. Empirical orthogonal functions and related techniques in atmospheric science: a review. International Journal of Climatology, 27(9): 1119–1152, doi: 10.1002/joc.1499

Hayasaki M, Kawamura R, Mori M, et al. 2013. Response of extratropical cyclone activity to the Kuroshio large meander in northern winter. Geophysical Research Letters, 40(11): 2851–2855, doi: 10.1002/grl.50546

Holgate S J, Matthews A, Woodworth P L, et al. 2013. New data systems and products at the permanent service for mean sea level. Journal of Coastal Research, 29(3): 493–504, doi: 10.2112/JCOASTRES-D-12-00175.1

Kalnay E, Kanamitsu M, Kistler R, et al. 1996. The NCEP/NCAR 40-year reanalysis project. Bulletin of the American Meteorological Society, 77(3): 437–472, doi: 10.1175/1520-0477(1996)077<0437:TNYRP>2.0.CO;2

Kawabe M. 1985. Sea level variations at the Izu Islands and typical stable paths of the Kuroshio. Journal of the Oceanographical Society of Japan, 41(5): 307–326, doi: 10.1007/BF02109238

Kawabe M. 1987. Spectral properties of sea level and time scales of Kuroshio path variations. Journal of the Oceanographical Society of Japan, 43(2): 111–123, doi: 10.1007/BF02111887

Kawabe M. 1995. Variations of current path, velocity, and volume transport of the Kuroshio in relation with the large meander. Journal of Physical Oceanography, 25(12): 3103–3117, doi: 10.1175/1520-0485(1995)025<3103:VOCPVA>2.0.CO;2

Kelly K A, Small R J, Samelson R M, et al. 2010. Western boundary currents and frontal air-sea interaction: Gulf Stream and Kuroshio Extension. Journal of Climate, 23(21): 5644–5667, doi: 10.1175/2010JCLI3346.1

Li Wei, Xie Yuanfu, He Zhongjie, et al. 2008. Application of the multigrid data assimilation scheme to the China Seas' temperature forecast. Journal of Atmospheric and Oceanic Technology, 25(11): 2106–2116, doi: 10.1175/2008JTECHO510.1

Li Rui, Zhang Zuowei, Wu Lixin. 2014. High-resolution modeling study of the Kuroshio path variations south of Japan. Advances in Atmospheric Sciences, 31(5): 1233–1244, doi: 10.1007/s00376-014-3230-4

Ma Libin. 2019. Response of ocean dynamics to multiple equilibria of the Kuroshio path south of Japan. Dynamics of Atmospheres and Oceans, 85: 57–71, doi: 10.1016/j.dynatmoce.2019.01.001

Mellor G L, Häkkinen S M, Ezer T, et al. 2002. A generalization of a sigma coordinate ocean model and an intercomparison of model vertical grids. In: Pinardi N, Woods J, eds. Ocean Forecasting: Conceptual Basis and Applications. Berlin, Heidelberg: Springer, 55–72, doi: 10.1007/978-3-662-22648-3_4

Mitsudera H, Taguchi B, Waseda T, et al. 2006. Blocking of the Kuroshio large meander by baroclinic interaction with the Izu ridge. Journal of Physical Oceanography, 36(11): 2042–2059, doi: 10.1175/JPO2945.1

Mitsudera H, Waseda T, Yoshikawa Y, et al. 2001. Anticyclonic eddies and Kuroshio meander formation. Geophysical Research Letters, 28(10): 2025–2028, doi: 10.1029/2000GL012668

Miyama T, Miyazawa Y. 2013. Structure and dynamics of the sudden acceleration of Kuroshio off Cape Shionomisaki. Ocean Dynamics, 63(2–3): 265–281, doi: 10.1007/s10236-013-0591-7

Miyazawa Y, Kagimoto T, Guo Xinyu, et al. 2008. The Kuroshio large meander formation in 2004 analyzed by an eddy-resolving ocean forecast system. Journal of Geophysical Research: Oceans, 113(C10): C10015, doi: 10.1029/2007JC004226

Miyazawa Y, Yamane S, Guo Xinyu, et al. 2005. Ensemble forecast of the Kuroshio meandering. Journal of Geophysical Research: Oceans, 110(C10): C10026, doi: 10.1029/2004JC002426

Nakamura H, Nishina A, Minobe S. 2012. Response of storm tracks to bimodal Kuroshio path states south of Japan. Journal of Climate, 25(21): 7772–7779, doi: 10.1175/JCLI-D-12-00326.1

Nakamura H, Yamashiro T, Nishina A, et al. 2006. Time-frequency variability of Kuroshio meanders in Tokara Strait. Geophysical Research Letters, 33(21): L21605, doi: 10.1029/2006GL027516

Nakata H, Funakoshi S, Nakamura M. 2000. Alternating dominance of postlarval sardine and anchovy caught by coastal fishery in relation to the Kuroshio meander in the Enshu-nada Sea. Fisheries Oceanography, 9(3): 248–258, doi: 10.1046/j.1365-2419.2000.00140.x

Nitani H. 1975. Variation of the Kuroshio south of Japan. Journal of the Oceanographical Society of Japan, 31(4): 154–173, doi: 10.1007/BF02107107

North G R, Bell T L, Cahalan R F, et al. 1982. Sampling errors in the estimation of empirical orthogonal functions. Monthly Weather Review, 110(7): 699–706, doi: 10.1175/1520-0493(1982)110<0699:SEITEO>2.0.CO;2

Qiu Bo, Chen Shuiming. 2005. Variability of the Kuroshio Extension jet, recirculation gyre, and mesoscale eddies on decadal time scales. Journal of Physical Oceanography, 35(11): 2090–2103, doi: 10.1175/JPO2807.1

Qiu Bo, Miao Weifeng. 2000. Kuroshio path variations south of Japan: bimodality as a self-sustained internal oscillation. Journal of Physical Oceanography, 30(8): 2124–2137, doi: 10.1175/1520-0485(2000)030<2124:KPVSOJ>2.0.CO;2

Sekine Y, Fujita K. 1999. Why does the sea level difference between Kushimoto and Uragami show periods of large meander and non-large meander paths of the Kuroshio south of Japan?. Journal of Oceanography, 55(1–2): 43–51, doi: 10.1023/A:1007857005988

Solomon H. 1978. Occurrence of small "trigger" meanders in the Kuroshio off southern Kyushu. Journal of the Oceanographical Society of Japan, 34(3): 81–84, doi: 10.1007/BF02109256

Song Tao, Wang Zihe, Xie Pengfei, et al. 2020. A novel dual path gated recurrent unit model for sea surface salinity prediction. Journal of Atmospheric and Oceanic Technology, 37(2): 317–325, doi: 10.1175/JTECH-D-19-0168.1

Sugimoto S, Hanawa K. 2012. Relationship between the path of the Kuroshio in the south of Japan and the path of the Kuroshio Extension in the east. Journal of Oceanography, 68(1): 219–225, doi: 10.1007/s10872-011-0089-1

Sugimoto T, Ishimaru T, Kobayashi M. 1986. Circulation and water

exchange in the anticyclonic gyre off Shikoku. Deep-Sea Research Part A: Oceanographic Research Papers, 33(11–12): 1641–1652, doi: 10.1016/0198-0149(86)90071-3

Sugimoto S, Qiu B, Kojima A. 2020. Marked coastal warming off Tokai attributable to Kuroshio large meander. Journal of Oceanography, 76(2): 141–154, doi: 10.1007/s10872-019-00531-8

Taft B A. 1972. Characteristics of the flow of the Kuroshio south of Japan. In: Stommel H, Yoshida K, eds. Kuroshio—Its Physical Aspects. Tokyo, Japan: University of Tokyo Press, 165–216

Torrence C, Compo G P. 1998. A practical guide to wavelet analysis. Bulletin of the American Meteorological Society, 79(1): 61–78, doi: 10.1175/1520-0477(1998)079<0061:APGTWA>2.0.CO;2

Tsujino H, Nishikawa S, Sakamoto K, et al. 2013. Effects of large-scale wind on the Kuroshio path south of Japan in a 60-year historical OGCM simulation. Climate Dynamics, 41(9–10): 2287–2318, doi: 10.1007/s00382-012-1641-4

Usui N. 2019. Progress of studies on Kuroshio path variations south of Japan in the past decade. In: Nagai T, Saito H, Suzuki K, et al., eds. Kuroshio Current: Physical, Biogeochemical, and Ecosystem Dynamics. Washington, D. C., USA: American Geophysical Union, 147–161, doi: 10.1002/9781119428428.ch9

Usui N, Tsujino H, Fujii Y, et al. 2006. Short-range prediction experiments of the Kuroshio path variabilities south of Japan. Ocean Dynamics, 56(5–6): 607–623, doi: 10.1007/s10236-006-0084-z

Usui N, Tsujino H, Nakano H, et al. 2008. Formation process of the Kuroshio large meander in 2004. Journal of Geophysical Research: Oceans, 113(C8): C08047, doi: 10.1029/2007JC004675

Usui N, Tsujino H, Nakano H, et al. 2011. Decay mechanism of the 2004/05 Kuroshio large meander. Journal of Geophysical Research: Oceans, 116(C10): C10010, doi: 10.1029/2011JC007009

Usui N, Tsujino H, Nakano H, et al. 2013. Long-term variability of the Kuroshio path south of Japan. Journal of Oceanography, 69(6): 647–670, doi: 10.1007/s10872-013-0197-1

Wang Jia, Oey L Y. 2014. Inter-annual and decadal fluctuations of the Kuroshio in East China Sea and connection with surface fluxes of momentum and heat. Geophysical Research Letters, 41(23): 8538–8546, doi: 10.1002/2014GL062118

Wang Jia, Oey L Y. 2016. Seasonal exchanges of the Kuroshio and shelf waters and their impacts on the shelf currents of the East China Sea. Journal of Physical Oceanography, 46(5): 1615–1632, doi: 10.1175/JPO-D-15-0183.1

Wei Yanzhou, Huang Daji, Zhu Xiaohua. 2013. Interannual to decadal variability of the Kuroshio current in the East China Sea from 1955 to 2010 as indicated by *in-situ* hydrographic data. Journal of Oceanography, 69(5): 571–589, doi: 10.1007/s10872-013-0193-5

Xu Haiming, Tokinaga H, Xie Shangping. 2010. Atmospheric effects of the Kuroshio large meander during 2004–05. Journal of Climate, 23(17): 4704–4715, doi: 10.1175/2010JCLI3267.1

Yamagata T, Umatani S I. 1987. The capture of current meander by coastal geometry with possible application to the Kuroshio current. Tellus A: Dynamic Meteorology and Oceanography, 39(2): 161–169, doi: 10.3402/tellusa.v39i2.11749

Yamagata T, Umatani S I. 1989. Geometry-forced coherent structures as a model of the Kuroshio large meander. Journal of Physical Oceanography, 19(1): 130–138, doi: 10.1175/1520-0485(1989)019<0130:GFCSAA>2.0.CO;2

Yasuda T, Sakurai K. 2006. Interdecadal variability of the sea surface height around Japan. Geophysical Research Letters, 33(1): L01605, doi: 10.1029/2005GL024920

Zhang Qin, Wang Hui, Dong Junyu, et al. 2017. Prediction of sea surface temperature using long short-term memory. IEEE Geoscience and Remote Sensing Letters, 14(10): 1745–1749, doi: 10.1109/LGRS.2017.2733548